Macromolecular Rapid Communications
www.mrc-journal.de

Semi-Transparent Luminescent Solar Concentrators Based on Intramolecular Energy Transfer in Polyurethane Matrices

*Elisavet Tatsi, Matteo De Marzi, Luca Mauri, Alessia Colombo, Chiara Botta, Stefano Turri, Claudia Dragonetti, and Gianmarco Griffini**

Luminescent solar concentrators (LSCs) are spectral conversion devices offering interesting opportunities for the integration of photovoltaics into the built environment and portable systems. The Förster-resonance energy transfer (FRET) process can boost the optical response of LSCs by reducing energy losses typically associated to non-radiative processes occurring within the device under operation. In this work, a new class of FRET-based thin-film LSC devices is presented, in which the synthetic versatility of linear polyurethanes (PU) is exploited to control the photophysical properties and the device performance of the resulting LSCs. A series of luminescent linear PUs are synthesized in the presence of two novel bis-hydroxyl-functionalized luminophores of suitable optical properties, used as chain extenders during the step-growth polyaddition reaction for the formation of the linear macromolecular network. By synthetically tuning their composition, the obtained luminescent PUs can achieve a high energy transfer efficiency (≈90%) between the covalently linked luminophores. The corresponding LSC devices exhibit excellent photonic response, with external and internal photon efficiencies as high as ≈4% and ≈37%, respectively. Furthermore, their optimized power conversion efficiency combined with their enhanced average visible-light transmittance highlight their suitability for potential use as transparent solar energy devices.

1. Introduction

In the vast realm of solar energy technologies, luminescent solar concentrators (LSCs) have gained popularity in the past decade as an interesting concept to enable the penetration of photovoltaic (PV) systems in the built environment as well as in some niche market segments where lightness, shape versatility and color tunability may represent important assets.[1] Despite significant potential, the practical deployment of LSCs has been hampered by their perceived underperformance attributable to various optical pathway losses, including incident light transmittance yielding reduced photon-absorption efficiency, poor photon trapping leading to photon escape at the LSC surfaces, and reabsorption of emitted photons limiting the device quantum yield.[2–6] These processes have led to power-producing LSC systems exhibiting device efficiencies in the 0.31–1.24% range.[7–11]

To address these challenges, the Förster resonance energy transfer (FRET) process has been proposed as a means to enhance the overall efficiency of LSCs by reducing energy losses due to non-radiative processes.[12–15] FRET is a process whereby the transfer of energy between two luminogens occurs through non-radiative dipole–dipole coupling, by placing an acceptor (emitter) molecule in close proximity to a donor (absorber) molecule and by enabling the energy transfer from the excited donor molecule to the acceptor molecule, the latter being responsible for the ultimate photon emission.[16,17]

Traditional approaches to implement FRET in LSC devices have been focused on the non-covalent incorporation of the FRET pair in the lightguide material (most commonly, an optically clear polymer such as polymethylmethacrylate – PMMA) in a host–guest fashion. Some recent examples of this type include small-molecule or π-conjugated-polymer pairs,[18–20] aggregation-induced-emission luminophores,[21–23] dendrimeric structures[24,25] and nanoparticle-based hybrid systems,[26,27] in some cases in the presence of a photoactive host matrix taking part in the FRET process.[28–30] In this device configuration, a key role is played by the photophysical characteristics of the luminophores and by their concentration in the host matrix, the latter influencing their average intermolecular distance, identified by the so-called critical FRET radius R_0, which should be in the 2–6 nm range for optimal interaction.[17,31]

Alternative strategies for FRET-based LSC systems have targeted the covalent incorporation of one or more luminophores within the macromolecular structure of the host matrix. This

E. Tatsi, M. De Marzi, S. Turri, G. Griffini
Department of Chemistry
Materials and Chemical Engineering "Giulio Natta"
Politecnico di Milano
Piazza Leonardo da Vinci 32, Milano 20133, Italy
E-mail: gianmarco.griffini@polimi.it
L. Mauri, A. Colombo, C. Dragonetti
Department of Chemistry
Università degli Studi di Milano
Via Camillo Golgi 19, Milano 20133, Italy
C. Botta
Institute of Sciences and Chemical Technologies "Giulio Natta" (SCITEC) of CNR
via Corti 12, Milano 20133, Italy

DOI: 10.1002/marc.202300724

bottom–up concept allows for efficient energy transfer between neighboring molecules via optimized donor–emitter intermolecular distancing, while offering the additional advantage of improving the solubility of the luminophore into the host matrix. This latter aspect is key to hamper molecular aggregation and minimize aggregation-caused luminescence quenching phenomena of the emission, by improving at the same time luminophore dispersion into host matrices, leading to reported device efficiencies of ≈0.5%.[11,32,33] In this context, a particularly interesting approach was proposed by Davis et al., consisting in intramolecular FRET systems with donor and emitter moieties grafted on the same polymer backbone.[34] In these acrylate-based polymeric structures, the polymer backbone was shown to act as a neutral scaffold providing controllable spacing between the pendant luminescent moieties, ultimately reducing molecular aggregation and enhancing the emissive properties of the overall system. In addition, judicious control of the polymer architecture by the introduction of non-luminescent spacers within the macromolecular network (namely, methyl methacrylate and tert-butyl acrylate) could effectively enhance the photoluminescence (PL) quantum yield (PLQY) of the FRET system.[35]

Despite the large body of work related to the application of the FRET concept to LSC devices in the past decade,[13,36,37] only very recently attempts were made to identify general guidelines to rationally design FRET-based LSC systems so as to achieve optimized performance. Among these, the maximization of the spectral overlap of the donor–emitter couple, the enhancement of the PLQY of both donor and emitter luminophores, the minimization of the intermolecular distance between the FRET pair, and the control of luminophore positioning and alignment within the host matrix were recognized as the most critical design factors for maximized optical performance of LSC devices.[13]

Following these important considerations, a new class of FRET-based thin-film LSC devices is presented in this work, in which the synthetic versatility of linear polyurethane (PU) networks is exploited to control the photophysical properties and the device performance of the resulting LSC system. In particular, departing from recent demonstrations of the application of this relatively unexplored class of polymeric materials as potential lightguide matrices in conventional host–guest LSCs,[38] this study reports on the development of a series of luminescent linear PUs via the "prepolymer approach",[39,40] to be used as photoactive elements in FRET-based LSC devices. To target an efficient FRET mechanism, two novel hydroxyl-functionalized luminescent molecules of suitable optical properties were designed and synthesized, namely 4,7-di(4-hydroxymethyl-phenyl)benzo(c)(1,2,5)thiadiazole (bHPBT) and 1,6,7,12-tetrakis(4-tert-butylphenoxy)-*N*, *N*′-(5-hydroxypentyl)-perylene-3,4,9,10-tetracarboxdiimide (bHPDI). These two functional luminophores were used in different proportions as chain extenders during the step-growth polyaddition reaction for the formation of linear luminescent PU macromolecular structures of tunable composition, photophysical characteristics, and FRET behavior (**Figure 1**). The photonic and PV responses of the resulting PU-based LSC devices were extensively characterized and useful structure–property-device performance correlations were demonstrated, proving the successful applicability of such materials in the area of highly-transparent spectral conversion devices.

2. Results and Discussion

2.1. Synthesis of Donor (bHPBT) and Acceptor (bHPDI) Luminophores

The luminescent FRET pair system presented in this work relies on the combination of 4,7-di(4-hydroxymethyl-phenyl)benzo(*c*)(1,2,5)thiadiazole (bHPBT) as donor and 1,6,7,12-tetrakis(4-*tert*-butylphenoxy)-*N*, *N*′-(5-hydroxypentyl)-perylene-3,4,9,10-tetracarboxdiimide (bHPDI) as acceptor. These two fluorescent diols were obtained starting from commercially available 4,7-dibromobenzo(c)(1,2,5)thiadiazole and 3,4,9,10-perylenetetracarboxylic dianhydride. The synthetic approaches to obtain such compounds were adapted from previously published procedures,[41–45] as reported in **Scheme 1** and **Scheme 2**.

2.2. Synthesis of Clear and Luminescent Polyurethane Systems

The clear and luminescent polyurethane systems were synthesized via the "prepolymer method" through a step-growth polyaddition under mild conditions. The NCO-terminated prepolymer was obtained by reaction of a fixed molar ratio (1:0.5) of isophorone diisocyanate (IPDI) and macromolecular diol (polyethylene glycol – PEG). The subsequent chain-extension process was performed by the addition of the short-chain diols (1.5 mol). In this step, 1,2-propanediol only was used to obtain the reference clear polyurethane material (referred to as PU). Furthermore, three additional groups of luminescent polymers were also synthesized: donor-only, acceptor-only, and donor–acceptor systems. In donor-only luminescent materials, both 1,2-propanediol and bHPBT were used as chain-extenders in different relative molar proportions, namely 1, 1.25, and 1.5 mol% (the resulting donor-only luminescent polymers will be referred to as D*x*, with $x = 1, 1.25, 1.5$ indicating the molar percent of the donor, bHPBT). In acceptor-only materials, bHPBT (donor) was replaced by bHPDI (acceptor) as additional low-molecular-weight diol in the chain-extension process together with 1,2-propanediol, at increasing molar concentrations: 0.1, 0.2, and 0.4 mol% (the resulting acceptor-only luminescent polymers will be referred to as PU-A*y*, with $y = 0.1, 0.2, 0.4$ indicating the molar percent of bHPDI – acceptor). Finally, in the donor–acceptor systems both bHPBT and bHPDI were used in combination with 1,2-propanediol as chain extenders. In this case, different proportions of the two luminescent diols were used, systematically increasing the molar concentration of the acceptor species, namely 7.5, 15, 30 mol% of bHPDI versus bHPBT, with bHPBT:bHPDI = 1:0.075, 1:0.15, 1:0.30 mol mol^{-1} (the donor molar concentration was fixed to that corresponding to the donor-only system with the highest dye concentration – PU-D1.5). The final donor–acceptor polymers will be noted as PU-DA*z*, with $z = 7.5, 15, 30$ indicating the molar percent of bHPDI versus bHPBT. The complete list of all synthesized polyurethane formulations (both clear and luminescent) is reported in **Table 1** (synthetic details can be found in the Experimental Section). As the chain-extension process involved different diols, the resulting polymer products was a complex mixture of macromolecules, with each chain containing a statistical array of coupled segments. The chemical structures of the building blocks used for the preparation

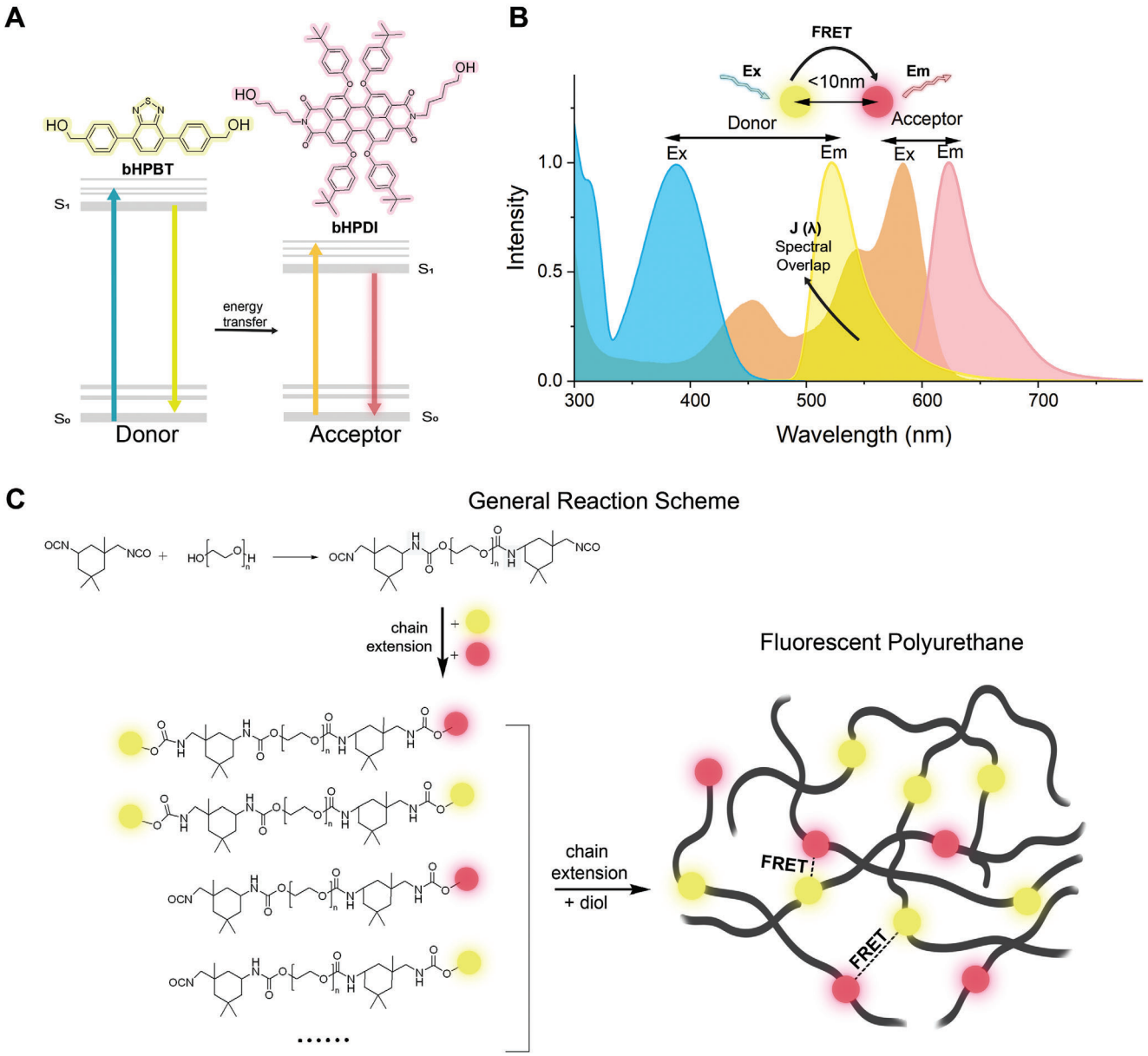

Figure 1. A) 4,7-di(4-hydroxymethyl-phenyl)benzo(c)(1,2,5)thiadiazole (bHPBT) and 1,6,7,12-tetrakis(4-tert-butylphenoxy)-*N*, *N*′-(5-hydroxypentyl)-perylene-3,4,9,10-tetracarboxdiimide (bHPDI) donor-acceptor pair; paradigm of the donor–acceptor excited states; B) absorption and emission spectra of the donor and acceptor molecule in solution (THF), with a focus on the FRET distance between the donor–acceptor pair and the spectral overlap between the emission of the donor and the absorption of the acceptor; C) general reaction scheme of luminescent polyurethanes and resulting macromolecules, with each chain containing a statistical array of coupled segments; representation of polyurethane macromolecular chains containing the luminescent molecules randomly localized, with indication of FRET mechanism.

of the final polymers and a possible sequence in a representative multiblock polyurethane system are shown in Figure 1C.

Prior to the incorporation of the luminescent small-molecular-weight diols, a preliminary study on the effect of the chain-length of the macromolecular diol used for the preparation of the pre-polymer on the glass transition temperature (T_g) and on the molecular weight (M_n) of the resulting clear PU materials was performed. This allowed us to define the most suitable precursor to be used in view of the final application in LSC devices. To that end, PEG macrodiols of different molecular weights were tested, namely 300, 600, 1000, and 2000 g mol^{-1} (PEG300, PEG600, PEG1000, and PEG2000, respectively).

As expected, successful covalent incorporation of the macrodiol units into the polyurethane chain could be evidenced by FTIR analysis, irrespective of the PEG chain length (Figure S10A, Supporting Information). In particular, the Fourier-transform infrared (FTIR) spectra evidenced the presence of signals typically associated with characteristic vibrations of —OH (3513 cm^{-1}), N—H (3333 and 1539 cm^{-1}), —CH_2 (2882 cm^{-1}), C=O (1702 cm^{-1}), C=C (1602, 1508, and 1468 cm^{-1}), C—N

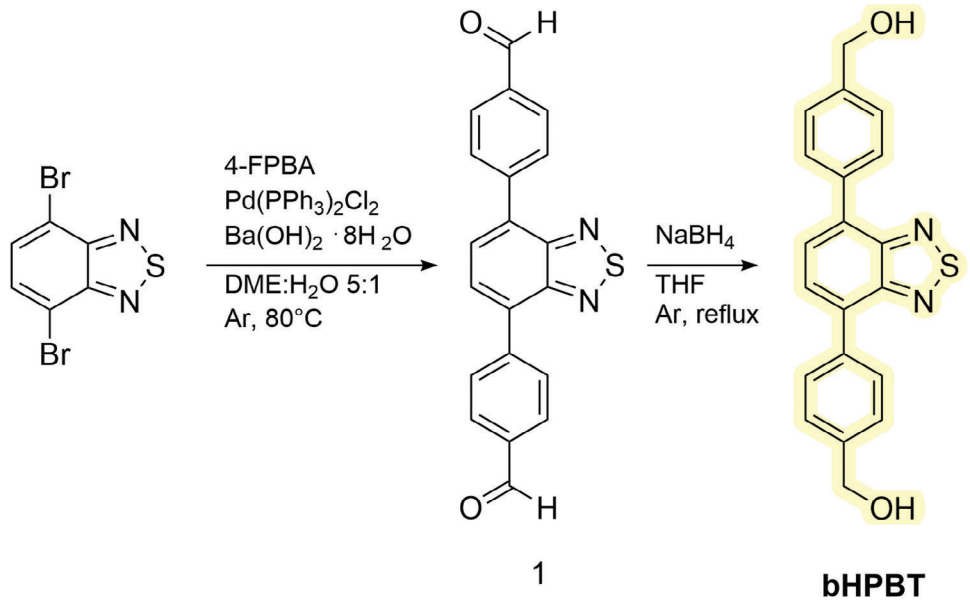

Scheme 1. Synthetic pathway for the preparation of the fluorescent diol bHPBT: A) 4-Formylphenylboronic acid (4-FPBA), $Pd(PPh_3)_2Cl_2$, $Ba(OH)_2 \cdot 8H_2O$, 1,2-Dimethoxyethane: H_2O 5:1, Ar, 80 °C, 24 h, B) $NaBH_4$, dry THF, Ar, reflux, 20 h.

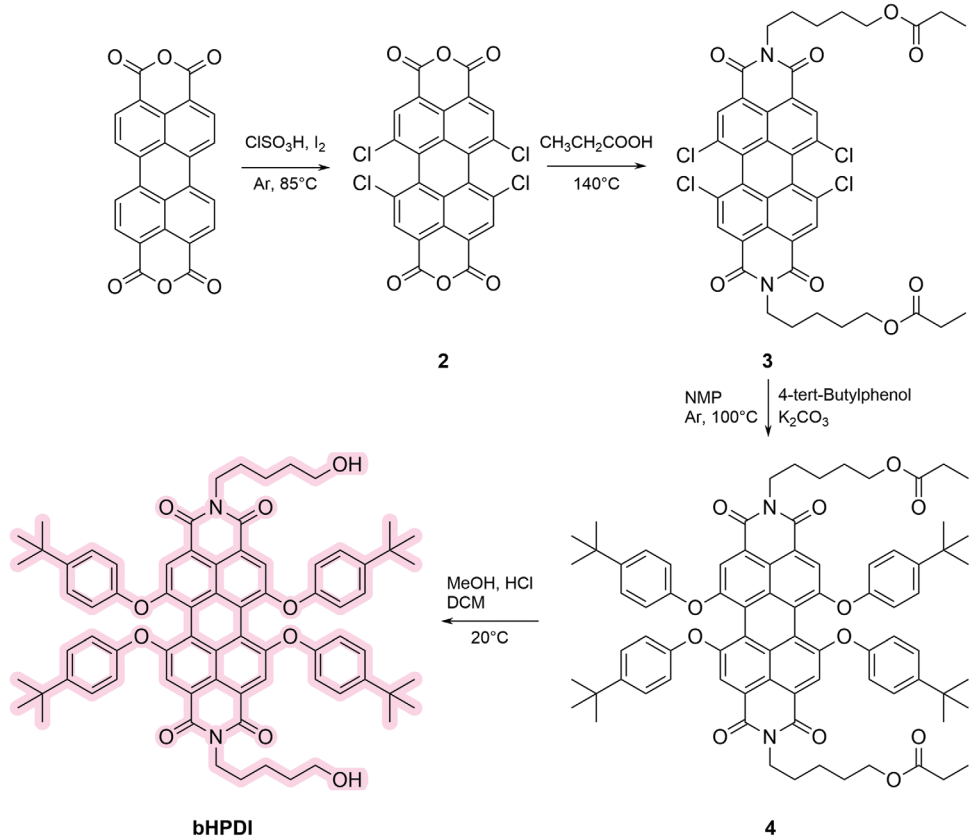

Scheme 2. Synthetic pathway for the preparation of the fluorescent diol bHPDI: A) $ClSO_3H$, I_2, Ar, 85 °C, 5 h, B) CH_3CH_2COOH, 140 °C, 24 h, C) 4-tert-Butylphenol, K_2CO_3, NMP, Ar, 100 °C, 24 h, D) MeOH, HCl 6 м, DCM, 20 °C, 48 h.

Table 1. Feed molar ratios and molecular weight (M_n) of all synthesized polyurethanes.

Sample	Donor bHPBT	Acceptor bHPDI	IPDI	PEG	1,2propanediol	M_n [g mol^{-1}]
PU-PEG300	-	-	1	0.5	1.5	3330
PU-PEG600	-	-	1	0.5	1.5	3120
PU-PEG1000	-	-	1	0.5	1.5	3080
PU-PEG2000	-	-	1	0.5	1.5	3110
PU-D1	0.0150	-	1	0.50[a)]	1.485	2770
PU-D1.25	0.0187	-	1	0.5[a)]	1.481	2470
PU-D1.5	0.0225	-	1	0.5[a)]	1.477	2400
PU-A0.1	-	0.00169	1	0.5[a)]	1.498	2970
PU-A0.2	-	0.00337	1	0.5[a)]	1.497	2930
PU-A0.4	-	0.00675	1	0.5 [a)]	1.494	3520
PU-DA7.5	0.0255	0.00169	1	0.5[a)]	1.473	3720
PU-DA15	0.0255	0.00337	1	0.5[a)]	1.470	3950
PU-DA30	0.0255	0.00675	1	0.5[a)]	1.466	3180

[a)] PEG300; [b)] PEG600; [c)] PEG1000; [d)] PEG2000.

(1310 cm^{-1}), C—H (1412, 1340, 1280, and 1235 cm^{-1}), and C—C (956 and 843 cm^{-1}) bonds, which were consistent with the expected chemical structure of the resulting PU.[46–48] Similarly, the complete disappearance of the signals attributed to N═C═O stretching vibrations (2267 cm^{-1}) in IPDI further confirmed the successful reaction of the isocyanate groups to form the PU network.

The optical properties (*viz.*, the transparency) of clear PUs were also found to be unaffected by the macrodiol chain-length, as in all cases high (95%) transmittance values over the entire visible spectrum could be recorded (Figure S13, Supporting Information).

On the contrary, varying the PEG chain length led to slight variations in the T_g of the clear PU materials, as inferred from differential scanning calorimetry (DSC). In particular, T_g values were found to increase from −20 °C in the case of PU obtained from high M_n PEG1000 and PEG2000, to ≈20 °C for PEG300 (Table S3, Supporting Information). Given the comparable values of obtained molecular weights, this effect can be attributed to the change in molecular mobility imparted by the relative lengths of soft segments and hard segments within the polyurethane network. In view of the ultimate application envisaged (LSC devices), PEG600, PEG1000, and PEG2000 were excluded as oligomeric precursors for the successive synthesis of luminescent materials, and all luminescent polymers (PU-D*x*, PU-A*y*, and PU-DA*z*) were obtained starting from PEG300 as macromolecular diol.

The feed compositions for all polyurethane material formulations are reported in Table 1, and were corroborated by ^{1}H NMR analysis performed on all synthesized polymers (see Supporting Information for all spectra and for the spectra evolution over time for a representative system, Figures S12, Supporting Information), confirming successful incorporation of luminescent precursors at all investigated molar ratios. Interestingly, no major variations in M_n were detected as a function of composition for the obtained luminescent systems, indicating no substantial effects on their chemical–physical response (Table 1).

2.3. Photophysics of Luminescent Polyurethane Thin-Films

The solid-state absorption and emission response of donor-only (PU-D*x*), acceptor-only (PU-A*y*), and donor-acceptor (PU-DA*z*) polyurethane materials were analyzed in thin-film configuration. Both front face and edge emission measurements were conducted to comprehensively analyze their emission behavior. The absorption and edge emission spectra of all systems are presented in **Figure 2**, while detailed information regarding front-face emission is provided in the Supporting Information (Figure S14, Supporting Information). All PU-D*x* systems possess an absorption spectrum extended to 450 nm with peak maxima at λ_{max1} = 278 nm and λ_{max2} = 387 nm, and display fluorescence emission between 400 and 650 nm, with an emission peak centered at 479 nm. Analogously, PU-A*y* materials are characterized by a broader absorption range extending up to 650 nm with peak maxima centered at λ_{max1} = 286 nm, λ_{max2} = 450 nm, and λ_{max3} = 577 nm Fluorescence emission for these systems ranges between 550 and 800 nm with a peak maximum at 620 nm. Notably, the emission spectra of solid-state PU-D*x* thin films exhibit a non-negligible blue-shift in comparison to the pristine dyes (bHPBT, bHDPI) dispersed in solution (see Figures S14,S15, Supporting Information). This shift can be attributed to the distinct chemical/solvation environment experienced by the dyes in the solid-state matrix.[34,49,50] Conversely, PU-A*y* films also display a slight blue-shift, albeit less pronounced than PU-Dx. Interestingly, both front-face and edge emission measurements reveal the same shape profiles and peak wavelengths, with a marginal red-shift observed for the LSCs measured in the edge-emission configuration. The corresponding absorption maxima and emission maxima for both edge and front-face emissions are provided in Table S5 (Supporting Information).

In what concerns PU-DA*z* systems (at varying bHPBT/bHPDI molar proportions) a noticeable increase in both absorption and fluorescence intensity is observed with increasing bHPDI (acceptor) content in the polyurethane formulation, specifically concerning the peaks associated with bHPDI. The peaks corresponding to bHPBT, on the other hand, remain constant, as expected.

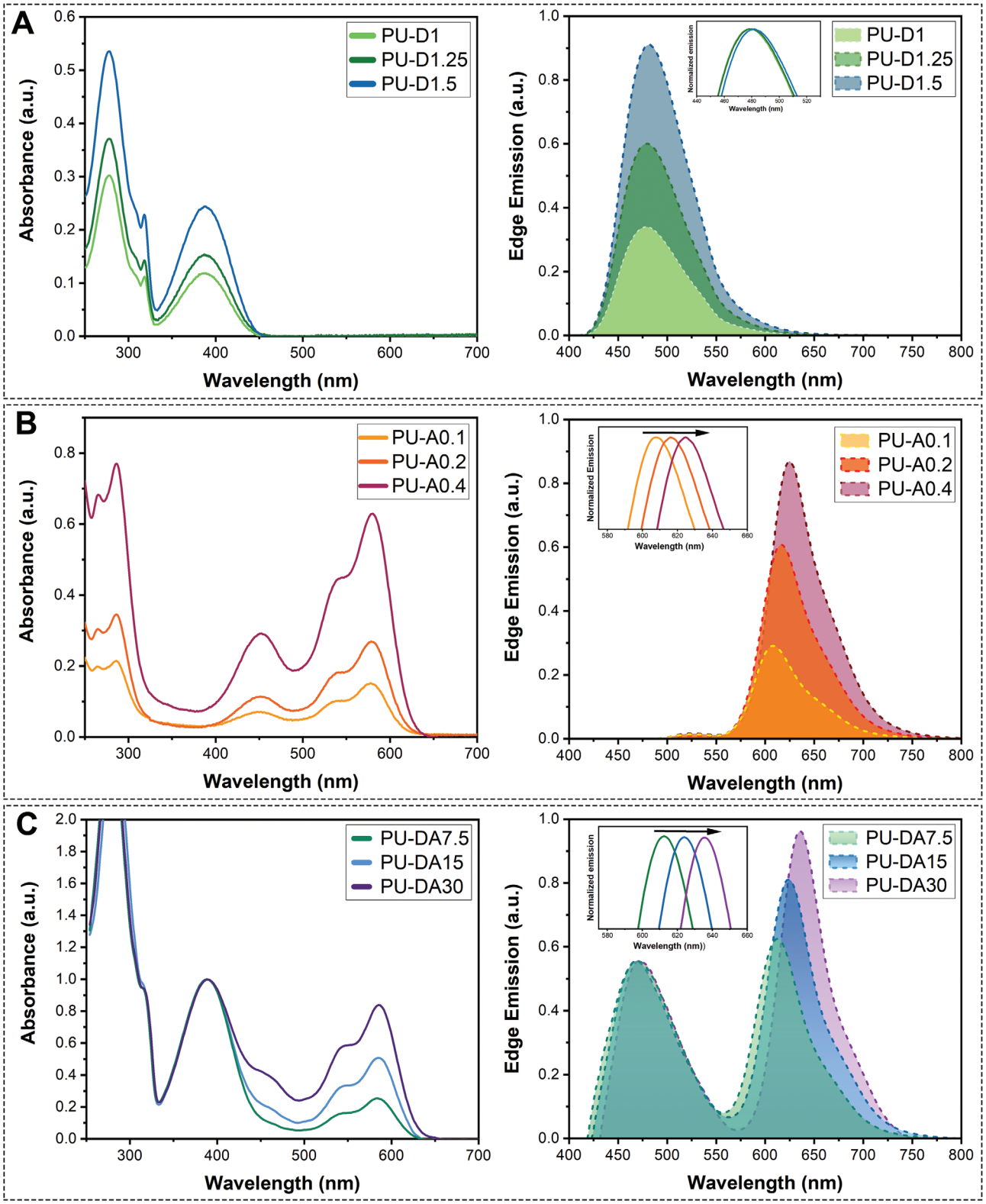

Figure 2. UV–vis and fluorescence spectra of A) donor-only (PU-D*x*), B) acceptor-only (PU-A*y*), and C) donor–acceptor (PU-DA*z*) polyurethane LSC systems. Excitation wavelength of the A) donor-only (PU-D*x*) was set at 384 nm, B) acceptor-only (PU-A*y*) was set at 450 nm, and C) donor–acceptor (PU-DA*z*) polyurethane was set at 384 nm.

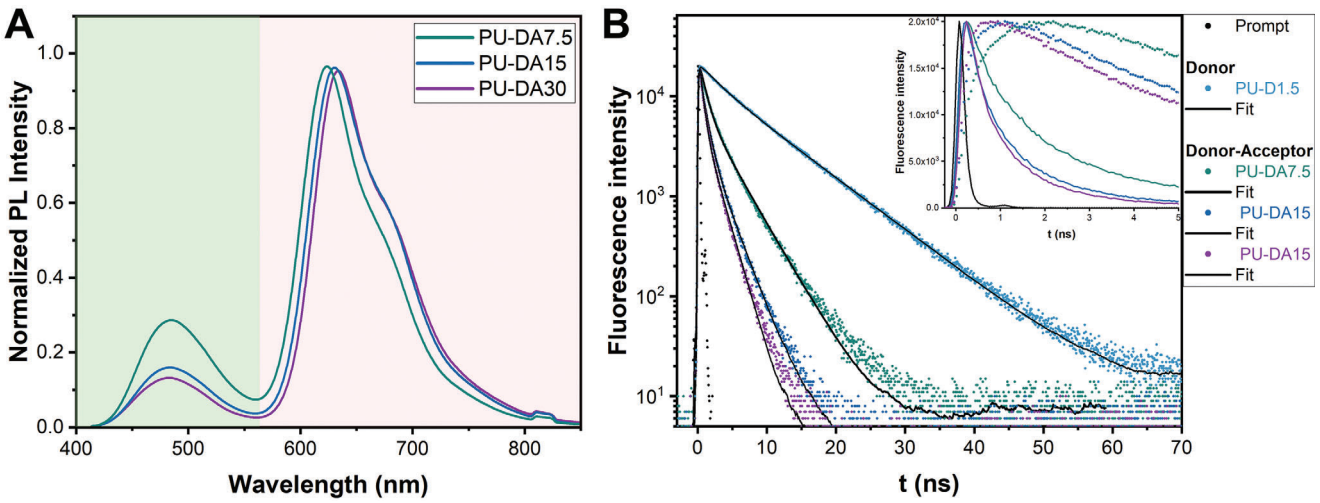

Figure 3. A) PL of PU-DA systems excited with a laser at 407 nm, B) emission decay (scatter plots) of the donor in PU-D1.5 and PU-DA systems as cast film (excitation 407 nm, emission at 482 nm, solid lines are biexponential fits). In the inset, an enlargement of the initial decay of PU-DA systems is reported for emissions at 482 nm (donor, solid lines) and 632 nm (acceptor, dashed lines).

In addition, both absorption and emission spectral profiles display the characteristic features of bHPBT and bHPDI molecules. In particular, three absorption peak maxima are found in all donor–acceptor polymers, centered at 279, 387, and 584 nm (Table S8, Supporting Information). Additionally, the emission spectra reveal two prominent bands peaking at λ_{max} = 468 nm and at λ_{max} = ≈620 nm, in line with the fluorescence characteristics of bHPBT and bHPDI, respectively. Differences between the relative emission intensities in PU-DA*z* systems become particularly evident as the bHPDI content is raised, leading to a progressive increase of the intensity of the band associated with bHPDI emission (575–725 nm), accompanied by a slight red-shift (from 612 nm in PU-DA7.5 to 627 nm in PU-DA30). Such changes in the fluorescence response with the increase in bHPDI content suggest that energy transfer between donor and acceptor moieties can successfully take place. First, the fluorescence intensity of bHPDI was found to increase (as discussed above), further confirming an effective donor–acceptor energy transfer process. Second, the fluorescence signal associated with the donor species (bHPBT) was shown to decline as the concentration of the acceptor species (bHPDI) increased in the donor–acceptor polymer, despite constant absorbance.

In order to gain a deeper understanding and quantitatively assess the energy transfer mechanisms within the PU-DA*z* polymeric systems, time-resolved fluorescence spectroscopy measurements were employed, by analyzing the fluorescence decay times (τ) of these materials in the solid state (Figure S17, Supporting Information). In **Figure 3** the emission decay of the donor in the absence of the acceptor (τ_D) (PU-D1.5) is compared with that of the donor in the presence of the acceptor (τ_{DA}) at different concentrations (PU-DA*z*). The lifetime (τ_{DA}) of the donor (bHPBT) in PU-DA*z* polymeric systems decreased with an increasing concentration of the acceptor (bHPDI), in accordance with an increasing quenching of the donor emission. More intriguingly, as evidenced in the inset of Figure 3B, upon 407-nm-laser excitation a clear rise of the acceptor emission intensity is observed in the first ns of the decays. The time rise of the acceptor emission is concentration dependent, in accordance with that of the donor quenching. This observation demonstrates that the donor quenching in the PU-DA*z* polymeric systems is associated to FRET to the acceptor.

To provide a deeper insight on the energy transfer process, its efficiency (η_{ET}) was estimated based on both fluorescence lifetimes and integrated donor and acceptor emissions (Equations S3,S4, Supporting Information) as detailed in the Supporting Information (Section S6, Supporting Information). The estimated values for all PU-DA*z* polyurethanes are presented in **Table 2**. Notably, the results evidence a progressive increase in the efficiency of the energy transfer process for increasing acceptor (bHPDI) concentration, leading to values as high as ≈90% for PU-DA30. To further evaluate the validity of our polyurethane donor-acceptor approach we also compared the PU-DA films with standard blends of PU-D and PU-A (Table S5, Supporting Information). The corresponding films displayed lower η_{ET} values, likely due to the presence of larger D–A distances, as expected in standard blended systems where micro-segregation often occurs.

2.4. Optical and Photovoltaic Characterization of Donor–Acceptor Luminescent Films

Based on the findings discussed thus far, thin-film LSC devices were fabricated on a laboratory scale (5.0 × 5.0 × 0.6 cm^3)[51] and subjected to colorimetry analyses to gauge their color perception under working conditions. To assess the visual appearance of the LSC, the Commission Internationale de l'Eclairage (CIE) 1931 *xy* coordinates system was utilized, which is the conventional method for evaluating materials under standard illumination. The transmitted light through PU-DA7.5, PU-DA15 and PU-DA30 exhibited CIE color coordinates of (x, y = 0.46, 0.34), (x, y = 0.56, 0.31) and (x, y = 0.59, 0.31), respectively. All devices achieved a color-rendering index above 95, while the correlated color temperature ranged from 1000 to 2000 K. These findings indicate minimal distortion in the transmitted light. Additionally,

Table 2. Photophysical properties of the luminescent polyurethane films: Fluorescence efficiency (Φ); Fluorescence maximum position (λ_{max}); the average lifetime of the donor (τ_D), acceptor (τ_A), and donor in the presence of the acceptor (τ_{DA}); Energy transfer efficiency (η_{ET}).

Sample	Φ[a)] [5–10% error]	λ^{max}[nm]	λ^{max}[nm]	τ_D [b)] [ns]	τ_A [c)] [ns]	τ_{DA} [b)] [ns]	η_{ET} [d)]
PU-D1.25	0.97	482	–	7.28			
PU-D1.5	1.00	482	–	7.00	--	-	-
PU-A0.1	0.37 [b)]	–	613	-	6.82	-	-
PU-A0.2	0.18 [b)]	–	624	-	7.30	-	-
PU-A0.4	0.19 [b)]	–	625	-	7.35	-	-
PU-DA7.5	0.54	484	622	-	-	1.75	0.76 [d)], 0.79 [e)]
PU-DA15	0.39	484	628	-	-	0.86	0.88 [d)], 0.88 [e)]
PU-DA30	0.33	482	632	-	-	0.73	0.90 [d)], 0.89 [e)]

[a)] λ_{exc} = 370 nm; [b)] λ_{exc} = 407 nm, λ_{em} = 482–484 nm; [c)] λ_{exc} = 407 nm, λ_{em} = 613–625 nm; [d)] $\eta_{ET} = 1 - \tau_{DA}/\tau_D$ with τ_D = 7 ns. $\tau = \Sigma i\ \alpha i \tau i$, from bi-exponential fits (see Equation S5, Supporting Information); [e)] η_{ET} = 1 − PLDA/PLD (see Equation S4, Supporting Information).

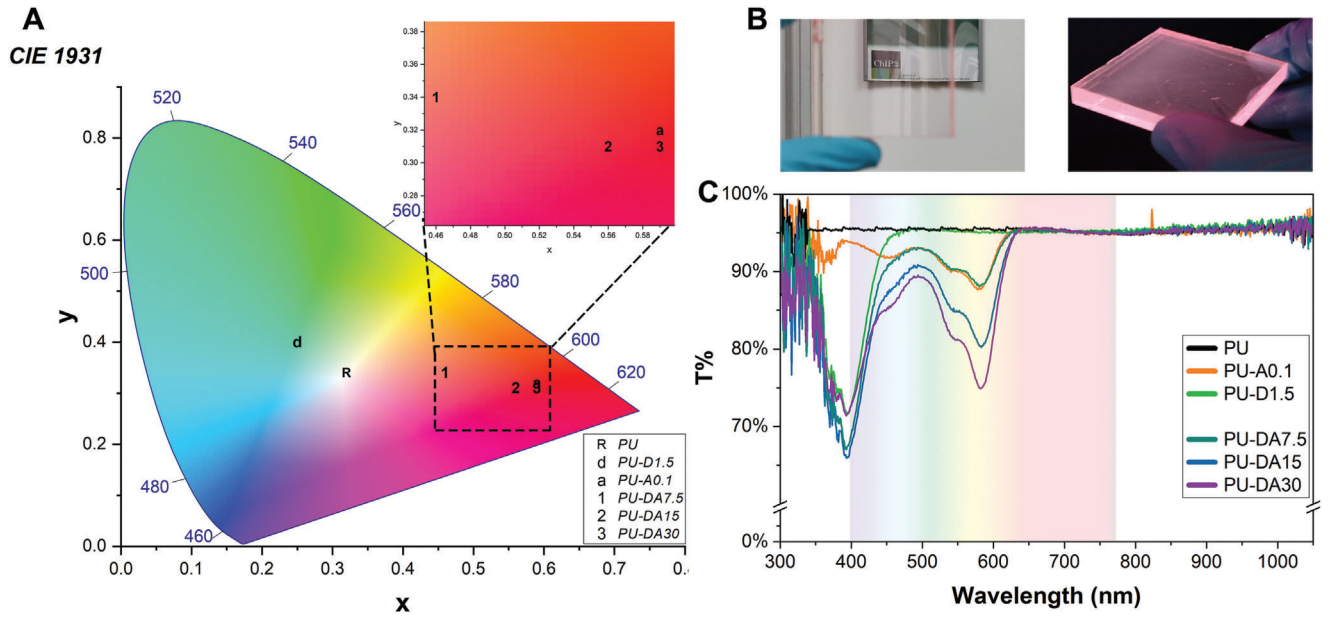

Figure 4. A) CIE 1931 color space chromaticity diagram reporting the color coordinates of the thin-film LSCs based on donor–acceptor PU-DAz polyurethanes. Additionally, color coordinates for transparent PU (R), PU-D1.5 (d), and PU-A0.1 (a) thin-film LSCs are provided for comparative analysis. B) Photographic images showcasing the PU-DA7.5 LSC device captured under both natural daylight and UV (366 nm) illumination conditions. C) Transmission spectra of donor–acceptor PU-DAz LSCs, alongside comparative spectra for transparent PU LSC (in black), PU-D1.5 LSC (in green), and PU-A0.1 LSC (in orange).

all coatings exhibited high transparency, as evidenced by the absence of haze or cloudiness in the visible light transmission spectra of all devices (see **Figure** 4B,C).

To evaluate the performance of thin-film LSCs based on donor–acceptor PU-DA polyurethane formulations as photonic devices, the single-edge optical power spectrum was recorded for each system under AM1.5G solar simulated irradiation (100 mW cm^{-2}), and two key parameters were calculated, namely, the external (η_{ext}) and the internal (η_{int}) photon efficiencies (Equations S6,S7, Supporting Information).

As depicted in **Figure** 5A, PU-DAz devices exhibited ηint values ranging from 27.5% to 37.5%, with PU-DA7.5 displaying the highest performance (η_{int} = 37.27%), followed by a subsequent decrease for higher acceptor-to-donor (bHPDI/bHPBT) ratios. This decay may be attributed to increasing quenching losses (non-radiative relaxation) taking place within the systems under these conditions. On the other hand, η_{ext} was shown to vary between 3.5% and 4%, with a peak response (η_{ext} = 3.97%) recorded for PU-DA15. Interestingly, these responses rank among the highest values reported in the literature for lab-scale devices of analogous spectral response tested under comparable light-exposure conditions.[52–55]

To evaluate the performance of the LSC-PV assembly based on PU-DA*z* systems, photocurrent measurements were also conducted by connecting two c-Si PV modules to opposite edges of the LSCs, and the power conversion efficiency (η_{dev}) was determined through PV measurements under AM1.5G simulated sunlight (100 mW cm^{-2}) illumination (see Equation S9, Supporting Information for details on the calculations), using a black absorbing background to avoid performance overestimation due

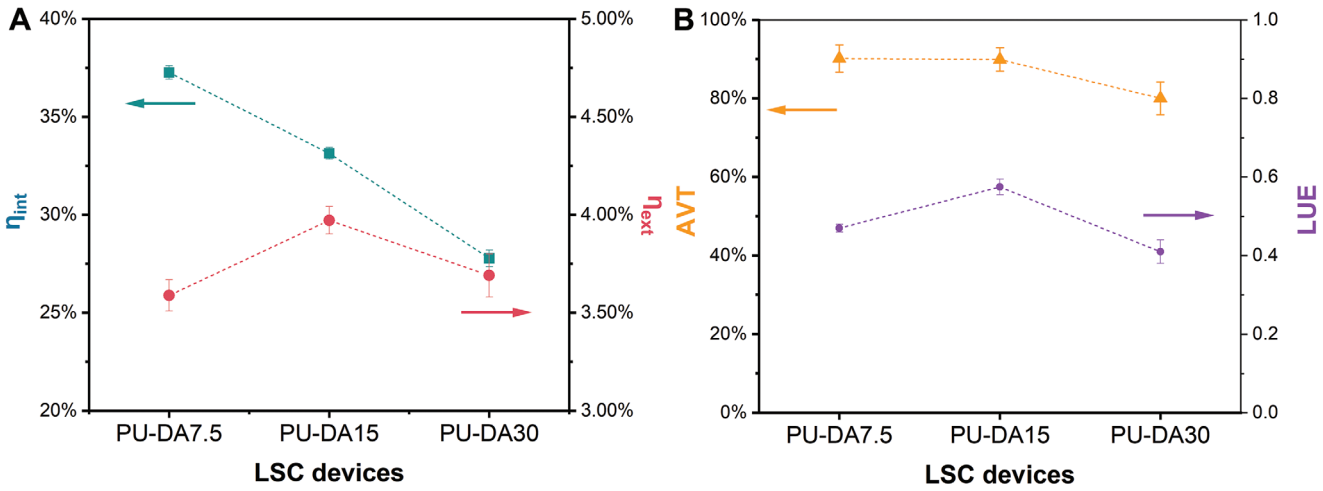

Figure 5. A) Internal (η_{int}) and external (η_{ext}) photon efficiencies, and B) AVT and LUE, for PU-DA-based LSC devices.

to double-pass of transmitted photons (experimental details and the comprehensive data collected, including V_{OC}, I_{SC}, FF, P_{max}, and η_{dev} for the different PU-DA LSC devices can be found in the Table S10, Supporting Information). In line with the results obtained from the photonic characterization discussed earlier, LSCs based on PU-DA15 were shown to exhibit the highest PV performance. In particular, a device efficiency η_{dev} as high as 0.64% could be obtained for this system, with a maximum I_{SC} of 8.98 mA and a maximum output power (P_{max}) of ≈20 mW.

To further assess the practical potential of such PU-DA systems for use as semi-transparent LSCs, and to facilitate the comparison with devices of different (higher) optical density (viz., luminophore concentration), the average visible-light transmittance (AVT) and the light utilization efficiency (LUE) were calculated (see Equations S10,S11, Supporting Information for details on the calculations).[56–58] The AVT assesses the transmittance of the devices based on the photopic response of the human eye, making such parameter particularly crucial for LSC application in buildings under sunlight illumination. As shown in Figure 5B, the AVT values for all PU-DA devices were found to range between ≈80% and ≈90%, with PU-DA30 exhibiting slightly lower transmittance given the higher concentration of acceptor (bHPDI) species. This behavior demonstrates that the high level of transmittance in the host matrix is preserved as neither haze nor cloudiness were detected, thus providing favorable arguments for the potential of these systems for building integration. Finally, the AVT was used in combination with the previously discussed η_{dev} to compute the LUE (=AVT × η_{dev}), which represents a more appropriate and holistic measure for comparing different devices in view of their applicability as transparent PV systems. As shown in Figure 5B, all PU-DA LSC devices exhibited LUE values between ≈0.25 and ≈0.7, in line with the most performing (semi)transparent LSC devices recently reported in the literature, ultimately demonstrating their potential for urban integration with minimal aesthetic impact.[59] Furthermore, to facilitate a thorough comparison between fabrication methods for FRET-based LSC devices, similar measurements were conducted for blend systems BLEND-PU*n*, with all relevant data provided in the Supporting Information. Analysis reveals that the copolymer approach, featuring in-chain covalently attached dyes, outperforms blending, in terms of photonic and photovoltaic efficiency based on higher values of internal and external efficiencies (η_{int} and η_{ext}) and PCE observed (Tables S9,S10, Supporting Information). Additionally, the AVT and LUE of blend systems are reported in Figure S21 (Supporting Information), indicating consistently high AVT values exceeding 80% across all systems. Furthermore, LUE values are lower for blend systems, reflecting their lower PCE compared to copolymers. Hence, the approach of incorporating in-chain covalently attached dyes appears to offer greater efficiency for FRET-based LSCs.

3. Conclusion

In this study, a new class of luminescent polyurethane systems were synthesized for application as thin films in high-performance LSC devices. Such materials were based on the covalent incorporation of novel luminescent diols in the polyurethane macromolecular structure, serving as in-chain donor and acceptor species for efficient FRET mechanism. Notably, the obtained luminescent polyurethanes demonstrated a high energy transfer efficiency (≈90%) between the donor and acceptor moieties. The corresponding LSC devices were shown to exhibit excellent photonic response, with external photon efficiency η_{ext} reaching up to ≈4% and internal photon efficiency η_{int} as high as ≈37%. Furthermore, their optimized power conversion efficiency η_{dev} combined with their enhanced average visible-light transmittance highlighted their suitability for potential use as transparent solar energy devices.

This work provides the first demonstration of LSCs exploiting the energy transfer mechanism through direct in-chain incorporation within luminescent polyurethane matrices, ultimately showing their potential in future building-integrated PV applications.

4. Experimental Section

Materials: 4,7-Dibromobenzo(c)(1,2,5)thiadiazole, 4-Formylphenyl boronic acid, $Pd(PPh_3)_2Cl_2$, 3,4,9,10-Perylenetetracarboxylic dianhydride,

Chlorosulfonic acid, $CDCl_3$ CD_3OD, Isophorone diisocyanate (IPDI), 1,2-propanediol, tetrahydrofuran (THF), anhydrous methanol, diethyl ether, dimethyl sulfoxide-d6 (d6-DMSO), were purchased from Sigma-Aldrich and used with no further purification. Polyethylene glycol (PEG) M_n ≈300, M_n ≈600, M_n ≈1000, and M_n ≈2000 were dehydrated by azeotropic distillation in toluene. Monocrystalline high-efficiency silicon solar cells were provided by IXYS (IXOLAR SolarBIT KXOB25-12 × 1F, active area = 2.2 × 0.6 cm^2, V_{OC} = 0.67 ± 0.01 V, J_{SC} = 53.60 ± 0.42 mA cm^{-2}, FF = 69.4 ± 0.3%, power conversion efficiency = 24.69 ± 0.23%).

Synthesis of 4,7-di(4-formyl-phenyl)benzo(c)(1,2,5)thiadiazole, 1: 4,7-Dibromobenzo(c)(1,2,5)thiadiazole (200.0 mg, 0.680 mmol), 4-Formylphenylboronic acid (305.9 mg, 2.040 mmol), $Pd(PPh_3)_2Cl_2$ (47.7 mg, 0.068 mmol), and $Ba(OH)_2 \cdot 8\ H_2O$ (643.5 mg, 2.040 mmol) were suspended in a mixture of 1,2-Dimethoxyethane (12.5 mL) and distilled water (2.5 mL). The reaction mixture was heated at reflux for 24 h under an argon atmosphere. After cooling to room temperature, dichloromethane was added, and the mixture was washed two times with distilled water. The organic phase was dried over Na_2SO_4 and evaporated under reduced pressure. The product was purified by flash chromatography on silica gel (eluent dichloromethane, then dichloromethane: MeOH 98:2) obtaining a pale-yellow solid (230.2 mg, 98.30%). ^{1}H-NMR: 400 MHz, $CDCl_3$, δ (ppm): 10.16 (2H, s), 8.21 (4H, d, J = 8 Hz), 8.10 (4H, d, J = 8 Hz), 7.94 (2H, s).

Synthesis of 4,7-di(4-hydroxymethyl-phenyl)benzo(c)(1,2,5)thiadiazole, bHPBT: 1 (430.3 mg, 1.249 mmol), and $NaBH_4$ (276.9 mg, 7.320 mmol) were suspended in dry THF (35 mL) and heated at reflux for 20 h under Ar atmosphere. After cooling to room temperature, the solvent was evaporated under reduced pressure, the obtained solid was suspended in distilled water (100 mL), stirred for 15 min, and isolated through vacuum filtration. The product was purified by flash chromatography on Al_2O_3 (eluent 95:5 dichloromethane: MeOH). The product was further purified by suspending it in Hex (10 mL), stirring the mixture at room temperature for 24 h, and isolating it through vacuum filtration. The product was a pale-yellow solid (298.3 mg, 68.55%). ^{1}H-NMR: 400 MHz, CD_3OD, δ (ppm): 8.04 (4H, d, J = 8 Hz), 7.91 ppm (2H, s), 7.55 (4H, d, J = 8 Hz), 4.73 (4H, s).

Synthesis of 1,6,7,12-Tetrachloro-3,4:9,10-perylene dianhydride, 2: In a 500 mL three-neck round-bottom flask equipped with a condenser and two glass stoppers, Perylene-3,4,9,10-tetracarboxylic dianhydride (2.0 g, 5.098 mmol) and I_2 (340.0 mg, 1.340 mmol) were dissolved in chlorosulfonic acid ($ClSO_3H$, 20.0 mL, 300.893 mmol), and the resulting mixture was heated at 85 °C for 5 h under N_2 atmosphere. After cooling to room temperature, the mixture was carefully dripped in a 1:1 distilled water: ice mixture, and the formed precipitate was collected by vacuum filtration and washed with distilled water until pH 6. The product was an orange-red solid (2.637 g, 4.975 mmol, 97.58%). ^{1}H-NMR: 400 MHz, D_2O + NaOD 40% in D_2O (5 drops), δ (ppm): 7.44 (4H, s).

Synthesis of 1,6,7,12-tetrachloro-N, N′-(pentyl-propanoate)-perylene-3,4,9,10-tetracarboxdiimide, 3: 2 (700.0 mg, 1.320 mmol), and 5-Amino-1-pentanol (680.9 mg, 6.600 mmol) were suspended in propanoic acid (12.0 mL) and heated at 140 °C for 24 h. After cooling to room temperature, the mixture was diluted with ethyl acetate (60 mL), put under stirring, and a saturated $NaHCO_3$ aqueous solution (200 mL) was slowly added. The phases were separated, and the organic phase was washed with distilled water three times, dried over Na_2SO_4, and concentrated under a vacuum. The product was isolated by flash chromatography on silica gel (eluent dichloromethane: AcOEt, from 35:1 to 20:1), obtaining a bright red-orange solid (740.3 mg, 0.911 mmol, 69.02%). ^{1}H-NMR: 300 MHz, $CDCl_3$, δ (ppm): 8.59 ppm (4H, s), 4.16 ppm (4H, t, J = 6 Hz), 4.06 ppm (4H, t, J = 6 Hz), 2.29 ppm (4H, q, J = 6 Hz), 1.71 ppm (8H, m), 1.47 ppm (4H, m), 1.09 ppm (6H, t, J = 6 Hz).

Synthesis of 1,6,7,12-tetrakis(4-tert-butylphenoxy)-N, N′-(pentyl-propanoate)-perylene-3,4,9,10-tetracarboxdiimide, 4: 3 (100 mg, 0.123 mmol), 4-*tert*-Butylphenol (128.7 mg, 0.857 mg), and K_2CO_3 (59.2 mg, 0.428 mmol) were suspended in dry NMP (7 mL). The resulting mixture was heated at 100 °C for 24 h under an Ar atmosphere. After cooling, 2 M HCl (20 mL) was added, and the product was extracted with AcOEt. The organic phase was washed twice with distilled water and brine dried over Na_2SO_4, and concentrated under reduced pressure. The raw product was used for the following reaction step without further purification.

Synthesis of 1,6,7,12-tetrakis(4-tert-butylphenoxy)-N, N′-(5-hydroxypentyl)-perylene-3,4,9,10-tetracarboxdiimide, 5: 4, MeOH (3.2 mL, 79.001 mmol), 6 M HCl (aq.) (100 µL, 0.600 mmol) and dichloromethane (5.0 mL) were stirred at room temperature in a 50 mL single-neck round-bottom flask for 48 h. The solvents were evaporated under reduced pressure and the resulting solid was dissolved in AcOEt (50 mL). The mixture was washed with a saturated $NaHCO_3$ aqueous solution and three times with distilled water dried over Na_2SO_4, and evaporated under vacuum. The product was isolated by flash chromatography on silica gel (eluent dichloromethane: AcOEt from 19:1 to 4:1). The product was a dark violet solid (54.8 mg, 0.047 mmol, 38.56%). ^{1}H-NMR: 300 MHz, $CDCl_3$, δ (ppm): 8.23 ppm (4H, s), 7.25 ppm (8H, d, J = 9 Hz), 6.85 ppm (8H, d, J = 9 Hz), 4.14 ppm (4H, t, J = 6 Hz), 3.63 ppm (4H, t, J = 6 Hz), 1.74 ppm (4H, quint, J = 6 Hz), 1.63 ppm (4H, m), 1.47 ppm (4H, m), 1.31 ppm (36H, s).

Synthesis of clear polyurethane systems: Initially, IPDI (4.5 mmol) was degassed under vacuum for 40 min at 70 °C in a three-neck bottom flask, after which the temperature was lowered to 60 °C and nitrogen gas was introduced. Pre-dried PEG (2.25 mmol) was mixed with anhydrous tetrahydrofuran (THF) and dibutyltin dilaurate (DBTDL, 44.99 µmol), and was then purged with nitrogen to remove oxygen and moisture prior to being added dropwise to the flask over a period of ≈30 min. The reaction was then left at 60 °C under vigorous stirring and under a nitrogen flux for 3 h to obtain the prepolymer. The reaction was monitored using FTIR and ^{1}H NMR (Figures S10–S12, Supporting Information). After 3 h, the chain extender (1,2-propanediol) was added to the prepolymer at a stoichiometric ratio of NCO/OH = 1:2. The mixture was then allowed to react under stirring at 60 °C in a static nitrogen atmosphere until all NCO groups were reacted (as inferred from FTIR and ^{1}H-NMR). The final polymer was washed with ethyl ether and placed in a Teflon container to be dried in a vacuum oven overnight.

Synthesis of luminescent polyurethane systems: For the synthesis of the luminescent polyurethane systems, bHPBT and bHPDI fluorescent diols were mixed with THF and DBTDL, and then loaded together dropwise into the reaction mixture at varying feed ratios (Table 1). The incorporation of the luminescent diols took place over a period of 1 h. Next, 1,2-propanediol (purged with nitrogen) was added dropwise into the system at a stoichiometric ratio of NCO/OH 1:2, in the presence of THF and DBTDL catalyst. The mixture was left stirring at 60 °C under static nitrogen until all NCO groups were reacted (as inferred by FTIR and ^{1}H-NMR). Prior to terminating the polymerization, dry methanol was added to the reaction to quench any unreacted NCO groups. The final polymer was washed with ethyl ether and placed in a Teflon container to be dried in a vacuum oven overnight.

Preparation of LSC in Thin-Film Configuration and LSC-PV Assembly: LSC devices were fabricated in thin/film configuration from luminescent polyurethanes solutions in THF at a fixed concentration of 30 wt.%. The obtained solution was spin-cast onto 5.0 × 5.0 × 0.6 cm^3 N-BK7 high-optical-quality glass windows using a Laurell WS-400BZ-6NPP/LITE instrument (900 rpm, 60 s; resulting film thickness ≈ 5 µm). LSC-PV devices were obtained by coupling two modules of two mc-Si solar cells each connected in series with two opposite edges of the glass substrate by means of ethyl-vinyl acetate hot melt adhesive (refractive index 1.49). The two remaining edges were left in contact with air.[51,60]

Characterization: ^{1}H NMR spectra at 400 MHz were recorded using deuterated chloroform as a solvent on a Bruker Avance 400 spectrometer. Gel permeation chromatography (GPC) analyses were carried out using a Waters 515 HPLC pump with THF operating at a flow rate of 1 mL min^{-1} and a temperature of 35 °C. Four Styragel columns (models HR 5, HR 4, HR 3, and HR 2) from Waters and a Waters 2410 refractive index detector were used. Samples were dissolved in THF at a concentration of 0.2 wt.%. A calibration curve was constructed using monodispersed fractions of polystyrene. FTIR spectra were obtained with a Jasco 660Plus instrument while the measurements were taken on solid films deposited on KBr windows, with 64 accumulated scans recorded at a resolution of 4 cm^{-1}. DSC analyses were carried out using a Mettler–Toledo DSC 823e instrument,

applying a thermal cycle consisting of heating from 0 to 150 °C, cooling from 150 to −50 °C, and reheating from −50 to 200 °C, with a heating rate of 20 °C min^{-1}. UV–vis absorption and transmission spectra were recorded on a Thermo Scientific Evolution 600 UV–vis spectrophotometer. Steady-state fluorescence spectroscopy analyses were performed on a Jasco FP-6600 spectrofluorometer on thin solid films, emission spectra of the samples were recorded in edge emission configuration.

PL and PL quantum yield (PLQY) were collected from the front face of the devices and they were carried out following the procedure reported elsewhere,[61] with NanoLog composed by an iH320 spectrograph equipped with a Synapse QExtra charge-coupled device, by exciting with a monochromate 450 W Xe lamp, or with a 405 nm Thorlabs DL5146-101S laser diode with LDC205C controller. The spectra were corrected for the instrument response. Time-resolved TCSPC measurements were obtained with PPD-850 single photon detector module by exciting with DD-405L DeltaDiode Laser and analyzed with the instrument Software DAS6.

Internal and external photon efficiency (η_{int} and η_{ext}, respectively) were assessed by illuminating the top face of the LSC using an Abet Technologies Sun 2000 solar simulator with AM1.5G filter (irradiance of 1000 W m^{-2}) and by collecting the edge-emitted photons of the LSC devices with a spectroradiometer (International Light Technologies ILT950) coupled with a cosine corrector.

Photovoltaic measurements were performed using a Keithley 2612B source-measuring unit, connected in series with the circuit, which imposed voltage scans and measured the current output. An absorbing black background in contact with the LSC rear side and a black mask on the front face of the LSC system were used in all experiments to prevent photon double-pass effects and direct illumination of the PV cells, respectively.

Supporting Information

Supporting Information is available from the Wiley Online Library or from the author.

Conflict of Interest

The authors declare no conflict of interest.

Data Availability Statement

The data that support the findings of this study are available from the corresponding author upon reasonable request.

Keywords

fluorescence, luminescent solar concentrators, perylene diimide, polyurethanes, resonance energy transfer, transparent photovoltaics

Received: February 23, 2024
Revised: March 12, 2024
Published online: March 23, 2024

[1] I. Papakonstantinou, M. Portnoi, M. G. Debije, *Adv. Energy Mater.* **2021**, *11*, 2002883.
[2] M. G. Debije, P. P. C. Verbunt, *Adv. Energy Mater.* **2012**, *2*, 12.
[3] B. McKenna, R. C. Evans, *Adv. Mater.* **2017**, *29*, 1606491.
[4] K. Park, J. Yi, S. Y. Yoon, S. M. Park, J. Kim, H. B. Shin, S. Biswas, G. Y. Yoo, S. H. Moon, J. Kim, M. S. Oh, A. Wedel, S. Jeong, H. Kim, S. J. Oh, H. K. Kang, H. Yang, C. J. Han, *Nat. Photonics* **2024**, *18*, 177.
[5] M. Bartolini, C. Micheletti, A. Picchi, C. Coppola, A. Sinicropi, M. Di Donato, P. Foggi, A. Mordini, G. Reginato, A. Pucci, L. Zani, M. Calamante, *ACS Appl. Energy Mater.* **2023**, *6*, 4862.
[6] A. Kathiravan, F. Mateen, P. Gopinath, D. Y. Hwang, S. K. Hong, S. M. H. Qaid, *Dyes Pigm.* **2024**, *222*, 111869.
[7] Y. Zhao, R. R. Lunt, *Adv. Energy Mater.* **2013**, *3*, 1143.
[8] Y. Zhao, G. A. Meek, B. G. Levine, R. R. Lunt, *Adv. Opt. Mater.* **2014**, *2*, 606.
[9] E. Tatsi, G. Fortunato, B. Rigatelli, G. Lyu, S. Turri, R. C. Evans, G. Griffini, *ACS Appl. Energy Mater.* **2020**, *3*, 1152.
[10] C. Yang, M. Moemeni, M. Bates, W. Sheng, B. Borhan, R. R. Lunt, *Adv. Opt. Mater.* **2020**, *8*, 1901536.
[11] A. Kaniyoor, B. McKenna, S. Comby, R. C. Evans, *Adv. Opt. Mater.* **2016**, *4*, 444.
[12] B. Zhang, P. Zhao, L. J. Wilson, J. Subbiah, H. Yang, P. Mulvaney, D. J. Jones, K. P. Ghiggino, W. W. H. Wong, *ACS Energy Lett.* **2019**, *4*, 1839.
[13] B. Zhang, G. Lyu, E. A. Kelly, R. C. Evans, *Adv. Sci.* **2022**, *9*, 2201160.
[14] J. Schiphorst, A. M. Kendhale, M. G. Debije, C. Menelaou, L. M. Herz, A. P. H. J. Schenning, *Chem. Mater.* **2014**, *26*, 3876.
[15] M. Carlotti, G. Ruggeri, F. Bellina, A. Pucci, *J. Lumin.* **2016**, *171*, 215.
[16] K. E. Sapsford, L. Berti, I. L. Medintz, *Angew. Chem., Int. Ed.* **2006**, *45*, 4562.
[17] J. R. Lakowicz, *Principles of Fluorescence Spectroscopy*, 3rd Ed., Springer, Baltimore, **2000**.
[18] G. D. Gutierrez, I. Coropceanu, M. G. Bawendi, T. M. Swager, *Adv. Mater.* **2016**, *28*, 497.
[19] J. E. A. Webb, K. Chen, S. K. K. Prasad, J. P. Wojciechowski, A. Falber, P. Thordarson, J. M. Hodgkiss, *Phys. Chem. Chem. Phys.* **2016**, *18*, 1712.
[20] G. Griffini, L. Brambilla, M. Levi, C. Castiglioni, M. Del Zoppo, S. Turri, *RSC Adv.* **2014**, *4*, 9893.
[21] J. L. Banal, K. P. Ghiggino, W. W. H. Wong, *Phys. Chem. Chem. Phys.* **2014**, *16*, 25358.
[22] B. Zhang, J. L. Banal, D. J. Jones, B. Z. Tang, K. P. Ghiggino, W. W. H. Wong, *Mater. Chem. Front.* **2018**, *2*, 615.
[23] B. Zhang, I. Lyskov, L. J. Wilson, R. P. Sabatini, A. Manian, H. Soleimaninejad, J. M. White, T. A. Smith, G. Lakhwani, D. J. Jones, K. P. Ghiggino, S. P. Russo, W. W. H. Wong, *J. Mater. Chem.* **2020**, *8*, 8953.
[24] O. A. Bozdemir, S. Erbas-cakmak, O. O. Ekiz, A. Dana, E. U. Akkaya, *Angew. Chem.* **2011**, *50*, 10907.
[25] N. J. L. K. Davis, R. W. MacQueen, S. T. E. Jones, C. Orofino-Pena, D. Cortizo-Lacalle, R. G. D. Taylor, D. Credgington, P. J. Skabara, N. C. Greenham, *J. Mater. Chem.* **2017**, *5*, 1952.
[26] C. S. Huang, K. Jakubowski, S. Ulrich, S. Yakunin, M. Clerc, C. Toncelli, R. M. Rossi, M. V. Kovalenko, L. F. Boesel, *Nano Energy* **2020**, *76*, 105039.
[27] A. R. Frias, E. Pecoraro, S. F. H. Correia, L. M. G. Minas, A. R. Bastos, S. García-Revilla, R. Balda, S. J. L. Ribeiro, P. S. André, L. D. Carlos, R. A. S. Ferreira, *J. Mater. Chem.* **2018**, *6*, 8712.
[28] G. Lyu, J. Kendall, I. Meazzini, E. Preis, S. Bayseç, U. Scherf, S. Clément, R. C. Evans, *ACS Appl. Polym. Mater.* **2019**, *1*, 3039.
[29] G. Fortunato, E. Tatsi, F. Corsini, S. Turri, G. Griffini, *ACS Appl. Polym. Mater.* **2020**, *2*, 3828.
[30] F. Corsini, C. M. Rizzini, C. Botta, S. Turri, G. Griffini, *Adv. Mater. Interfaces* **2022**, *9*, 2200108.
[31] N. Hildebrandt, in *FRET – Förster Resonance Energy Transfer*, Wiley, Weinheim, Germany, **2013**, pp, 105.
[32] A. R. Frias, R. A. S. Ferreira, R. Rondão, S. F. H. Correia, L. Fu, L. D. Carlos, S. J. L. Ribeiro, P. S. André, E. Pecoraro, *Adv. Sustainable Syst.* **2018**, *2*, 1800002.
[33] G. Lyu, T. J. F. Southern, B. L. Charles, M. Roger, P. Gerbier, S. Clément, R. C. Evans, *J. Mater. Chem.* **2021**, *9*, 13914.
[34] N. J. L. K. Davis, R. W. Macqueen, D. A. Roberts, A. Danos, S. Dehn, S. Perrier, T. W. Schmidt, *J. Mater. Chem.* **2016**, *4*, 8270.

[35] V. B. Yasarapudi, L. Frazer, N. J. L. K. Davis, E. P. Booker, A. Macmillan, J. K. Gallaher, D. Roberts, S. Perrier, T. W. Schmidt, *J. Mater. Chem.* **2018**, *6*, 7333.
[36] B. Balaban, S. Doshay, M. Osborn, Y. Rodriguez, S. A. Carter, *J. Lumin.* **2014**, *146*, 256.
[37] C. Tummeltshammer, M. Portnoi, S. A. Mitchell, A. T. Lee, A. J. Kenyon, A. B. Tabor, I. Papakonstantinou, *Nano Energy* **2017**, *32*, 263.
[38] P. Minei, G. Iasilli, G. Ruggeri, A. Pucci, *Shanghai Tuliao* **2020**, *10*, 655.
[39] M. F. Sonnenschein, *Polyurethanes: Science, Technology, Markets, and Trends*, John Wiley & Sons, Inc., Hoboken, New Jersey, **2014**.
[40] J. O. Akindoyo, M. D. H. Beg, S. Ghazali, M. R. Islam, N. Jeyaratnam, A. R. Yuvaraj, *RSC Adv.* **2016**, *6*, 114453.
[41] H. Dinçalp, Ş. Kizilok, S. Içli, *Dyes Pigm.* **2010**, *86*, 32.
[42] J. Qu, N. G. Pschirer, D. Liu, A. Stefan, F. C. De Schryver, K. Müllen, *Chem. - Eur. J.* **2004**, *10*, 528.
[43] A. Colombo, G. De Soricellis, F. Fagnani, C. Dragonetti, M. Cocchi, B. Carboni, V. Guerchais, D. Marinotto, *Dalton Trans.* **2022**, *51*, 12161.
[44] J. L. Wang, Z. M. Tang, Q. Xiao, Y. Ma, J. Pei, *Org. Lett.* **2008**, *10*, 4271.
[45] A. Shaygan Nia, C. Enders, W. H. Binder, *Tetrahedron* **2012**, *68*, 722.
[46] K. S. Liow, C. S. Sipaut, R. F. Mansa, M. C. Ung, S. Ebrahimi, *Polymers* **2022**, *14*, 3603.
[47] C. M. Gomez, D. Gutierrez, M. Asensio, V. Costa, A. Nohales, *J. Elastomers Plast.* **2017**, *49*, 77.
[48] X. Liu, W. Hong, X. Chen, *Polymers* **2020**, *12*, 2875.
[49] J. L. Banal, H. Soleimaninejad, F. M. Jradi, M. Liu, J. M. White, A. W. Blakers, M. W. Cooper, D. J. Jones, K. P. Ghiggino, S. R. Marder, T. A. Smith, W. W. H. Wong, *J. Phys. Chem. C* **2016**, *120*, 12952.
[50] L. Wang, C. Sun, S. Li, N. Jia, J. Li, F. Qu, K. Goh, Y. Chen, *Polymer* **2016**, *82*, 172.
[51] M. G. Debije, R. C. Evans, G. Griffini, *Energy Environ. Sci.* **2021**, *14*, 293.
[52] S. Mattiello, F. Corsini, S. Mecca, M. Sassi, R. Ruffo, G. Mattioli, Y. Hattori, T. Kusamoto, G. Griffini, L. Beverina, *Mater. Adv.* **2021**, *2*, 7369.
[53] F. Corsini, A. Nitti, E. Tatsi, G. Mattioli, C. Botta, D. Pasini, G. Griffini, *Adv. Opt. Mater.* **2021**, *9*, 2100182.
[54] L. Zdražil, S. Kalytchuk, K. Holá, M. Petr, O. Zmeškal, Š. Kment, A. L. Rogach, R. Zbořil, *Nanoscale* **2020**, *12*, 6664.
[55] N. S. Makarov, D. Korus, D. Freppon, K. Ramasamy, D. W. Houck, A. Velarde, A. Parameswar, M. R. Bergren, H. McDaniel, *ACS Appl. Mater. Interfaces* **2022**, *14*, 29679.
[56] C. Yang, D. Liu, R. R. Lunt, *Joule* **2019**, *3*, 2871.
[57] T. A. de Bruin, W. G. J. H. M. van Sark, *Front. Phys.* **2022**, *10*, 856799.
[58] C. J. Traverse, R. Pandey, M. C. Barr, R. R. Lunt, *Nat. Energy* **2017**, *2*, 849.
[59] J. Huang, J. Zhou, E. Jungstedt, A. Samanta, J. Linnros, L. A. Berglund, I. Sychugov, *ACS Photonics* **2022**, *9*, 2499.
[60] C. Yang, H. A. Atwater, M. A. Baldo, D. Baran, C. J. Barile, M. C. Barr, M. Bates, M. G. Bawendi, M. R. Bergren, B. Borhan, C. J. Brabec, S. Brovelli, V. Bulović, P. Ceroni, M. G. Debije, J.-M. Delgado-Sanchez, W.-J. Dong, P. M. Duxbury, R. C. Evans, S. R. Forrest, D. R. Gamelin, N. C. Giebink, X. Gong, G. Griffini, F. Guo, C. K. Herrera, A. W. Y. Ho-Baillie, R. J. Holmes, S.-K. Hong, T. Kirchartz, et al., *Joule* **2022**, *6*, 8.
[61] J. Moreau, U. Giovanella, J. P. Bombenger, W. Porzio, V. Vohra, L. Spadacini, G. Di Silvestro, L. Barba, G. Arrighetti, S. Destri, M. Pasini, M. Saba, F. Quochi, A. Mura, G. Bongiovanni, M. Fiorini, M. Uslenghi, C. Botta, *Chemphyschem* **2009**, *10*, 647.